PCCP

Accepted Manuscript

ROYAL SOCIETY OF CHEMISTRY

www.rsc.org/pccp

PCCP

RSCPublishing

ARTICLE

Two-dimensional electronic-vibrational spectra: modeling correlated electronic and nuclear motion

Cite this: DOI: 10.1039/x0xx00000x

F. Terenziani*[a] and A. Painelli[a]

Received ooth January 2012,
Accepted ooth January 2012

DOI: 10.1039/x0xx00000x

www.rsc.org/

We calculate 2D electronic-vibrational (2D-EV) spectra of solvated organic dyes modeled in terms of a reduced set of electronic diabatic states (the essential states) non-adiabatically coupled to molecular vibrations. An effective overdamped coordinate, whose dynamics is described by the Smoluchowski diffusion equation, accounts for polar solvation. Results are discussed for two dyes with distinctively different spectroscopic behavior: 4-(dicyanomethylene)-2-methyl-6-(4-dimethylaminostyryl)-4H-pyran (DCM) and 8-(N,N-dibutylamino)-2-azachrysene (AAC). Linear absorption and fluorescence spectra of DCM are well reproduced based on a minimal two-state model. The same model leads to 2D-EV spectra in good agreement with the recent experimental data by Oliver and coworkers for DCM in DMSO. On the opposite, linear spectra of AAC show a subtle interplay between a locally-excited (LE) and charge-transfer (CT) excitation, calling for a three-state model. Calculated 2D-EV spectra for AAC show a qualitatively different behavior, demonstrating that the experimental data for DCM do not support a LE/CT interplay. This resolves the long-lasting discussion about the nature of low-lying excitations of DCM in favor of the simplest picture.

Introduction

Two-dimensional (2D) optical spectroscopy is a powerful tool to investigate the excited-state dynamics of molecular and supramolecular systems following ultrafast excitation.[1–3] In 2D optical experiments, a pulse sequence creates an excited-state population, and a delayed pulse interrogates the system. Pulses in different spectral regions can be used, typically in the mid-infrared or in the visible-UV regions. 2D-IR spectra, collected using pump and probe beams in the mid-IR, provide transient structural information, including anharmonicities, vibrational mode coupling, as well as indirect information on energy- or charge-transfer rates and dynamics.[4,5] 2D electronic spectroscopy (2D-ES), using visible (or UV) pump and probe beams, provide instead detailed information about aggregates and multichromophoric assemblies, including electronic couplings, about exciton-exciton coherence and population transfers.[6–12]

Very recently, a new type of 2D optical spectroscopy has been introduced, the so-called 2D electronic-vibrational (2D-EV) spectroscopy, where a sequence of two visible pulses creates a population in the electronic (or better vibronic) excited state of the system, and a delayed IR probe pulse interrogates it.[13] The newly proposed 2D-EV spectroscopy offers a new perspective on the relaxation of photoexcited systems, governed by the subtle interplay of electronic and vibrational degrees of freedom.

Excited-state dynamics is governed by a variety of phenomena, including electronic and vibrational couplings, electron-phonon coupling, solvation and inhomogeneous broadening effects. Reliable models are therefore needed for a thorough understanding of 2D spectra, accounting for the different kinds of interactions.[2,14–17] In the past years, we contributed to develop essential-state models, a family of comparatively simple effective models that describe low-energy optical spectra of charge-transfer dyes. In particular, different models were developed for different families of charge-transfer dyes, from dipolar[18,19] to quadrupolar,[20,21] octupolar[22–24] and more complex structures,[25–27] by selecting a minimal electronic basis set (typically corresponding to the main resonance structures) and explicitly accounting for electron-vibration coupling and polar solvation. Essential-state models were successfully used to rationalize and quantitatively reproduce or predict several spectral properties, including steady-state absorption and fluorescence,[19–24,28] vibrational (IR and Raman) spectra,[28] time-resolved fluorescence and pump-probe spectra,[29] two-photon absorption,[20–23,30] hyper-Rayleigh,[24] etc. The models were applied to describe spectra of charge-transfer dyes in solution, in aggregates or supramolecular assemblies.[30–34]

Here, inspired by the recent experiment by Oliver et al.,[13] we extend the essential-state approach to calculate 2D optical

spectra, specifically 2D-EV spectra. This novel extension of the essential-state approach will be applied to two dyes that have been extensively investigated in our laboratory and whose spectral properties were successfully described by essential-state models of different complexity. The first species of interest is the laser dye 4-(dicyanomethylene)-2-methyl-6-(4-dimethylaminostyryl)-4H-pyran (hereafter DCM, Figure 1), whose 2D-EV spectra are reported by Oliver et al.,[13] allowing for a direct comparison with experiment. The second dye is 8-(N,N-dibutylamino)-2-azachrysene (hereafter AAC, Figure 1), whose 2D-EV spectra are not available yet but could be considered in future experiments. A joint experimental and theoretical study of AAC unambiguously proved that the low-energy spectral properties of AAC are governed by a subtle interplay between a locally-excited (LE) and a charge-transfer (CT) state, mainly driven by solvation.[27] The nature of low-energy excitations of DCM is instead more controversial. Some researchers invoke the presence of both a CT and a LE state,[35–38] other researchers instead support a picture where only the CT state plays a role.[19,39] In the past, we quantitatively reproduced absorption and fluorescence spectra, as well as transient electronic spectra of DCM, based on the "standard" two-state model.[19,29] Therefore, according to our analysis, DCM is a typical representative of polar (push-pull) dyes, whose lowest excitation has a well-defined CT character. Here, the detailed analysis of 2D-EV spectra calculated for the two dyes and a quantitative comparison with experimental data on DCM demonstrate that 2D-EV spectroscopy offers a deep insight into the electronic excited states of solvated molecules, easily discriminating the different nature of excitations and solving the old controversy about DCM in favor of the simplest picture.

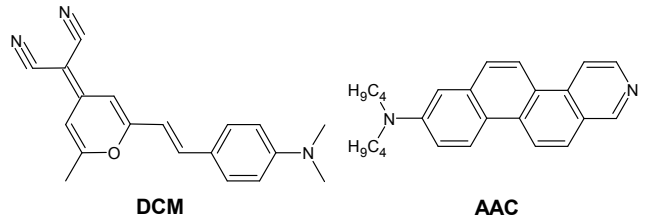

Figure 1. Molecular structures of the investigated dyes.

The model

The essential-state model for push-pull dyes with donor-π-acceptor (D-π-A) motif (where π is a conjugated bridge) accounts for just two electronic diabatic states, corresponding to the limiting valence-bond structures, D-π-A and D^+-π-A^-.[19] As schematically illustrated in Figure 2 (top-left panel), the two states are separated by an energy gap 2η, and are mixed by a matrix element $\langle D\text{-}\pi\text{-}A|H|D^+\text{-}\pi\text{-}A^-\rangle = -\tau$. The dipole moment of the D^+-π-A^- state, μ_0, is large, and other matrix elements of the dipole moment operator are neglected. To account for polar solvation, we introduce F, the electric reaction field generated at the location of the solute due to the reorientation of polar solvent molecules. F stabilizes D^+-π-A^-, so that the energy gap between the two diabatic states becomes $2\eta - \mu_0 F$. If the solute is described as a continuum elastic medium, an additional term, $(\mu_0 F)^2/(4\varepsilon_{or})$, enters the Hamiltonian to account for the elastic energy needed to create the field, where ε_{or} measures the solvent reorganization energy.[19]

At variance with many push-pull dyes, the spectra of AAC point to the presence of a second excited state lying close to the CT state.[27] Therefore, for AAC, the previous two-state model was extended to include a third diabatic state, D-π*-A, describing a local excitation.[27] This state is assigned an energy 2ζ and is coupled to the D^+-π-A^- state through the matrix element $\langle D\text{-}\pi^*\text{-}A|H|D^+\text{-}\pi\text{-}A^-\rangle = -\beta$ (for a sketch of the model, see Figure 2, top-right panel). The LE basis state has a negligible permanent dipole moment; in order to account for the finite intensity of the LE transition, we assign a finite value to $\langle D\text{-}\pi\text{-}A|\mu|D\text{-}\pi^*\text{-}A\rangle = \mu_*$.

In either model, F describes a slow motion and is dealt with in the adiabatic approximation. The diagonalization of the F-dependent electronic problem then leads to F-dependent eigenvalues, i.e. the adiabatic potential energy surfaces (PES)[19] as reported in Figure 2 (bottom panels, full lines). As a reference, the diabatic states are also shown as dashed lines. In push-pull dyes, the stabilization of the D^+-π-A^- basis state in polar solvents is responsible for the well-known

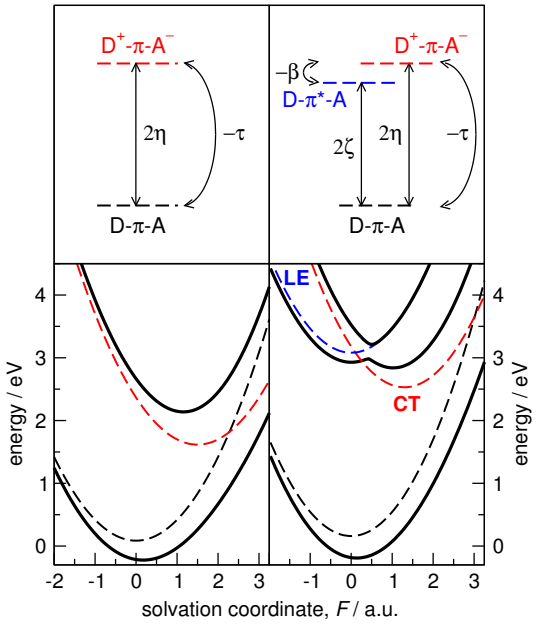

eigenstates (black full lines) as a function of the solvation coordinate.

To complete the models, we introduce an effective vibrational coordinate, Q, with corresponding frequency ω_v. The diabatic D-π-A and D^+-π-A^- states have displaced minima along Q, so

that the energy gap acquires a linear dependence on Q, namely $2\eta - \mu_0 F - \omega_v\sqrt{2\varepsilon_v}Q$, where ε_v is the vibrational relaxation energy.[19] In the three-level LE/CT model, a second vibrational coordinate, q, is introduced (with corresponding frequency ω_* and relaxation energy ε_*), linearly coupling the D-π-A and LE diabatic states.[27]

The adiabatic approximation safely applies to the solvation coordinate, but has to be carefully evaluated when dealing with vibrational motion. In fact, the adiabatic approximation is doomed to fail whenever the energy difference between the electronic states becomes comparable to the vibrational quanta, as it is the case for the LE/CT three-level model. We therefore rely on the direct diagonalization of the nonadiabatic Hamiltonian matrix, as described in the original literature.[20,27] Briefly, for fixed F values, the (F-dependent) Hamiltonian matrix is written on the basis obtained as the direct product of the electronic diabatic states and the eigenstates of the harmonic oscillators associated with each vibrational coordinate (one oscillator for the two-level model, two oscillators for the three-level model). The nominally infinite basis associated with each oscillator is truncated to the M lowest states. The Hamiltonian matrix is then diagonalized to get numerically exact vibronic eigenstates, provided M is large enough to get convergence ($M = 10$ is used here). Transition energies and transition and permanent dipole moments, as needed for optical spectra, are calculated from the eigenvectors. Steady-state optical spectra are finally obtained as sum of spectra obtained for different F-values, weighting each spectrum for the relevant Boltzmann distribution. Specifically, the ground-state Boltzmann distribution applies to absorption spectra while, for fluorescence spectra, the Boltzmann distribution must be calculated based on the energy of the emitting state.

The nonadiabatic approach is conceptually simple and applies smoothly even to difficult cases where large anharmonicities are present and/or several electronic states have similar energies. Its main drawback is that it hinders the classification of excited states as "vibrational" or "electronic": all the nonadiabatic eigenstates are in fact "vibronic". This is not an issue in the calculation of absorption spectra but, to calculate fluorescence spectra, the emissive state must be identified as the lowest excited state with *electronic character*. This is possible through a detailed analysis of the eigenvectors and/or a comparison of transition dipole moments from the ground state (electronic transitions are typically characterized by much bigger transition dipole moments than vibrational ones) or permanent dipole moments (CT states are characterized by large permanent dipole moments).[20,27]

Calculated absorption and fluorescence spectra for DCM and AAC in solvents of different polarity are reported in the Supporting Information (Figure S1), together with a short discussion. Calculated fluorescence spectra for DCM well reproduce the prominent evolution of the fluorescence bandshape with solvent polarity.[19] This evolution was often ascribed to a supposed variation of the nature of the fluorescent state from LE to CT.[35–37] We demonstrated instead that the minimal two-state model, with a pure CT excitation, fully accounts for this phenomenon,[19] but of course this does not exclude the presence of a low-lying LE state. Transient electronic spectroscopy could solve the controversy, but the analysis of transient spectra is hindered by the broad nature of the spectral features and by the partial overlap of transient stimulated emission and absorption bleaching.[35–37] These problems made it impossible to unambiguously identify the nature of the excited state of DCM. 2D-EV spectroscopy, following the dynamics over the excited-state PES by means of an IR probe, overcomes these drawbacks, offering detailed information about the nature of excited states.

Results and discussion

In the 2D-EV experiment (pump-probe configuration) a sequence of visible pulses creates an out-of-equilibrium population in the resonant excited state. A delayed IR pulse (or series of pulses) then addresses the spectral properties of the system while the population evolves towards the excited-state equilibrium.[13] Due to the finite spectral width of the pump pulse, only the vibronic excited states resonant with the beam profile can be reached. Just after excitation the instantaneous (vertical) occupation probability of the excited vibronic states for each value of the reaction field is given by the initial (ground-state) probability at the same value of the field, multiplied by the absorbance of the sample as induced by the specific pump-beam spectral profile. To mimic the experiment, we consider a pump beam with a Gaussian spectral shape with full width at half maximum of 950 cm^{-1} centered at 515 nm (19417 cm^{-1}) for DCM and 350 nm (28571 cm^{-1}) for AAC (see Figure S2, we remark that the results are marginally affected by the precise spectral position of the pump beam, as long as it falls within the absorption band).

After photoexcitation, vibrational coordinates relax in a very fast process, usually accomplished within the first few hundreds of femtoseconds. Solvation dynamics is much slower, occurring in a temporal window ranging from hundreds of femtoseconds to few picoseconds, depending on the solvent and on the specific solute. On this basis, it is possible to separate the vibrational and solvation motions, assuming that solvation dynamics starts after vibrational cooling.[40,41] Specifically, in the simulation of solvent dynamics, the vibrational relaxation is considered instantaneous, so that at the *effective zero time* of solvation[40] the nuclear degrees of freedom are already relaxed. In our simulation, the effective zero-time distribution is obtained by collapsing, for each F value, the excited-state population into the state responsible for steady-state emission. The resulting distribution is shown in Figure 3 as a full thick indigo line (labeled "0"). For comparison, in the same figure the dotted thin line shows the ground-state equilibrium distribution (labeled gs), while the thermally-equilibrated distribution relevant to the excited state is reported as a dashed red thick line (labeled relaxed). This relaxed distribution is calculated as the Boltzmann distribution relevant to the emissive state.

The evolution of the probability distribution from the effective zero time to the fully relaxed limit is calculated using the Smoluchowski diffusion equation:[42]

$$\frac{\partial w(F,t)}{\partial t} = \frac{1}{\tau_s}\left[w(F,t)\frac{\partial^2 V(F)}{\partial F^2} + \frac{\partial V(F)}{\partial F}\frac{\partial w(F,t)}{\partial F} + kT\frac{\partial^2 w(F,t)}{\partial F^2}\right]$$

where w is the F and t-dependent probability distribution, $V(F)$ is the PES governing the evolution, τ_s is the average solvation time (typical of each solvent),[43,44] k is the Boltzmann constant and T the temperature (set to 298 K). Consistently with the separation between nuclear and solvation dynamics, vibrational and electronic degrees of freedom are assumed to be always in equilibrium with the instantaneous configuration of the solvent.

Results about the evolution of the F-distribution with time, reported in Figure 3, are calculated setting $\tau_s = 3$ ps, as relevant to DMSO.[43,44] Calculated distributions are shown as thin full lines for selected delay times (specified by the labels). For the two-level model (panel a), the F-distribution evolves smoothly, progressively shifting and changing shape towards the equilibrium.

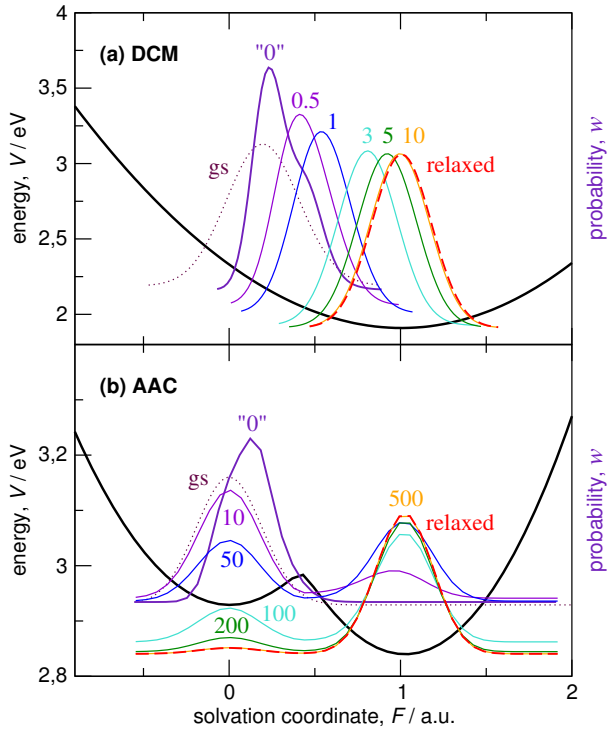

Figure 3. The energy of the emissive excited state (full black line) as a function of the solvation coordinate, calculated for DCM (panel a) and AAC (panel b), both in DMSO. The probability distribution of the solvation coordinate is reported for different pump-probe delay times (full lines of different colors, each labeled by the corresponding delay time, in ps, measured with respect to the effective zero time of solvation, labeled "0"). As a reference, the probability distributions of the solvation coordinate relevant to the ground state (dotted line labeled gs) and to the relaxed excited state (dashed red line labeled relaxed) are also reported.

The situation is qualitatively different for AAC (panel b), where the distribution evolves along a double-minimum PES. The zero-time distribution is centered in the region of the metastable LE-like minimum, and the evolution drives the system towards the thermodynamically stable minimum having mainly CT character. The dynamics involves the crossing of a barrier, whose height is approximately $2kT$. Accordingly, the dynamics is much slower than for a single-minimum PES: only after about 500 ps the distribution reaches the thermodynamic equilibrium.

Based on transient distributions, purely absorptive 2D-EV spectra are calculated as difference in the IR-absorbance (as measured by the probe beam) of the optically pumped transient system and the system at rest. The absorbance variation (ΔA) has positive contributions from excited-state absorption and negative contributions from ground-state bleaching and stimulated emission. 2D data are reported in Figs. 4 and 5 as color maps, showing ΔA as a function of the pump frequency, ω_{VIS}, in the visible region, and of the probe frequency, ω_{IR}, in the IR region.

2D-EV spectra calculated for DCM in DMSO according to the two-level model are shown in Figure 4, for different delay times, starting from the effective zero time of solvation. Since we introduce a single effective molecular vibration, the spectrum is less crowded than the experimental one and can be straightforwardly interpreted. Just accounting for vibrationally cool states, stimulated emission does not contribute in the IR spectral region (hot-states contributions are in any case expected to switch off in the first 100-200 fs). The observed negative (red) ΔA peak then corresponds to the ground-state absorption bleaching. Along the ω_{VIS} axis, the relevant signal is centered at the central frequency of the pump beam, while along the ω_{IR} axis it is centered at the ground-state vibrational frequency (1320 cm^{-1}). As expected, the position and shape of the bleaching signal are marginally time-dependent. The bleaching signal, in fact, is due to non-excited molecules and the residual time-dependence is related to the readjustment of the ground-state population after depletion (spectral diffusion effects, expressing as broadening along the ω_{IR} axis).

The excited-state absorption signal (blue peak, positive ΔA) shows instead an interesting temporal evolution, with the peak progressively moving towards higher frequencies along both the ω_{IR} and the ω_{VIS} axes. Concomitantly, the peak intensity increases. Both phenomena can be explained quite naturally as due the molecular polarizability, responsible for the readjustment of the electronic and vibrational structure in response to the instantaneous local solvation field.[29] At the effective zero time, electronic and vibrational degrees of freedom are in local equilibrium with the out-of-equilibrium zero-time distribution of the solvation coordinate. At later times, the distribution of the solvation coordinate evolves towards equilibrium, moving in a region of larger F, favoring a more effective mixing of the two resonating D-π-A and D^+-π-A^- forms. As it is well known from the early days of the two-state model,[18,28] as the mixing between the two states increases, the excited-state vibrational frequency hardens, and the intensity of vibrational transitions increases (see SI, Figure S3), thus

explaining the blue shift of the excited-state absorption signal along the ω_{IR} axis and the concomitant increase of intensity.

Understanding the evolution of the signal along the ω_{VIS} axis is more subtle. Before pumping, the solution can be described as a collection of slightly different molecules, each one in equilibrium with the local value of the reaction field.[19] Out of this inhomogeneous distribution of molecules, the visible pump selectively excites the sub-ensemble of molecules whose vibronic transition frequencies are resonant with the beam profile (photoselection).[28] Just after excitation, the IR probe addresses the specific photoselected sub-ensemble of molecules, and the excited-state absorption band is centered at the same ω_{VIS} position as the ground-state bleaching. Since the pump beam has a finite spectral width, by itself it photoselects an inhomogeneous sub-ensemble: in particular, the red side of the pump beam preferentially excites molecules with lower excitation energies, i.e. molecules characterized by a larger mixing of the two basis states and hence a larger dipolar character (see Figure S3 and relevant discussion); the blue side of the pump beam instead preferentially excites molecules having lower excitation energies, i.e. lower dipolar character. Following the excitation, the generated out-of-equilibrium distribution evolves, moving towards regions of larger F (see Figure 3) and photoselected molecules readjust their electronic and vibrational properties, accordingly. Out of the initially excited sub-ensemble, molecules having low polar character (those preferentially excited by the blue side of the pump beam) increase their polarity towards the equilibrium, with a consequent increase of their IR absorption. At the same time, photoexcited molecules with a higher dipolar character (those excited by the red side of the pump beam), being closer to the equilibrium, modify less their polar character, so that their IR absorption intensity is less affected. Therefore, as the system evolves towards the excited-state equilibrium, a stronger intensity increase is experienced by molecules excited by photons in the blue side of the pump beam with respect to molecules excited by red-side photons, leading to an apparent blue-shift of the excited-state absorption signal along the ω_{VIS} axis. The results shown for DCM in Figure 4 are indeed general: qualitatively similar behavior is expected for push-pull dyes, quite irrespective of model parameters.

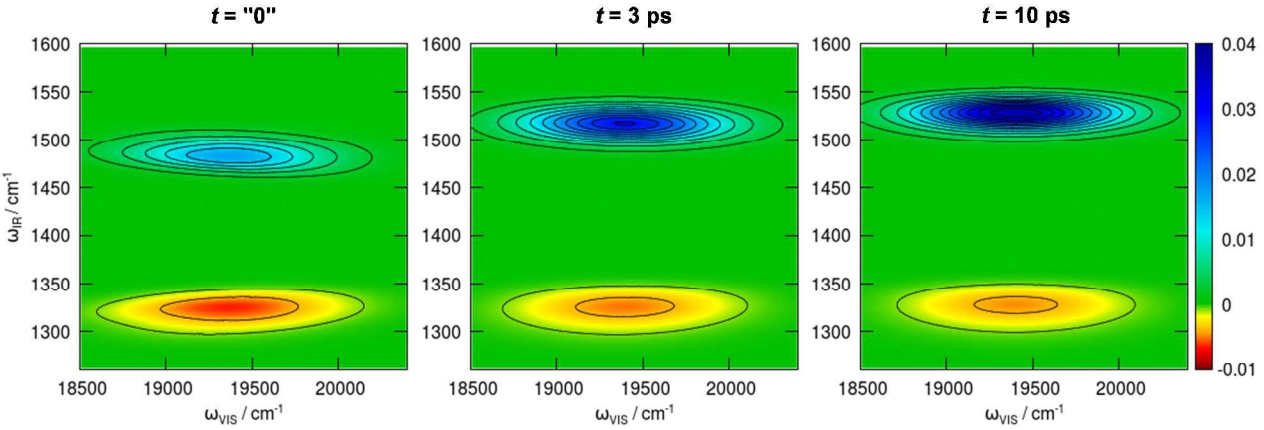

Figure 4. Purely absorptive 2D-EV spectra calculated for DCM in DMSO via the two-state model (parameters in Table S1), for the delay times reported on top of each panel. The color maps report the ΔA value according to the palette on the right (arbitrary units).

Maps representing the time evolution of the 2D-EV bands integrated over the ω_{VIS} axis or over the ω_{IR} axis are reported in Figure S4, while Figure S5 shows the time evolution of the average frequency calculated for the positive-ΔA peak along the ω_{VIS} and the ω_{IR} axes. Both curves can be fitted by monoexponential functions, with time constants (1.96 and 2.24 ps, respectively) comparable to the adopted solvation time. The 2D-EV spectrum calculated at zero time after excitation, before vibrational cooling, is shown in Figure S6. In this case, stimulated emission contributes to the signal. Moreover, the excited-state absorption band has slightly modified shape and intensity, but no significant shift is observed with respect to the zero time of solvation, along either the ω_{IR} or the ω_{VIS} axis. Therefore, vibrational cooling is marginally relevant in the evolution of the 2D-EV spectrum (at least in the case of a single vibrational mode).

The spectra calculated for DCM in the framework of the two-state model, reported in Figure 4, explain the main features of the experimental 2D-EV spectra,[13] namely the progressive intensity increase of the main excited-state-absorption band and its blue shift along the ω_{IR} and ω_{VIS} axes at increasing pump-probe delay times. Actually, the calculated shift along the ω_{IR} axis (~ 40 cm^{-1}) is somewhat overestimated (a result related to a well-known weakness of the model that overestimates the vibrational hardening of the excited state due to the lack of higher-energy electronic excited states),[29] while the shift along the ω_{VIS} axis (~ 20 cm^{-1}) is underestimated. The obtained agreement is however impressive, demonstrating the reliability and predictive capabilities of the model, that was proposed and parameterized for DCM more than 10 years ago, based on steady-state absorption and fluorescence spectra.[19] Unfortunately, experimental 2D-EV spectra do not cover the

spectral region relevant to the ground-state frequency of the most coupled mode.

In order to definitely rule out the LE/CT interplay in DCM, we now address 2D-EV spectra of AAC. As discussed above, a three-state model has been proposed for this molecule where clear signatures of competing LE and CT states are evident already in steady-state absorption and emission spectra.[27] 2D-EV spectra calculated for AAC in DMSO, for selected time delays, are reported in Figure 5 (see also Figure S7). The spectra are qualitatively different from those obtained for DCM. First of all, the dynamics for AAC is much slower that for DCM, even if the same solvation time is adopted. Indeed, in AAC, to move from the initial LE-like state to the final CT-like state, a barrier must be overcome, whose height affects the dynamics: simulations run on PES with a lower barrier lead to faster dynamics. On the other hand, the shape of the PES and the height of the barrier only marginally affect the shape of calculated 2D-EV spectra. In particular (see Figure 5), the excited-state absorption feature (positive ΔA) is always very broad along the ω_{IR} axis (please notice the wide spectral region along the ω_{IR} axis), showing two main peaks along that axis at early times.

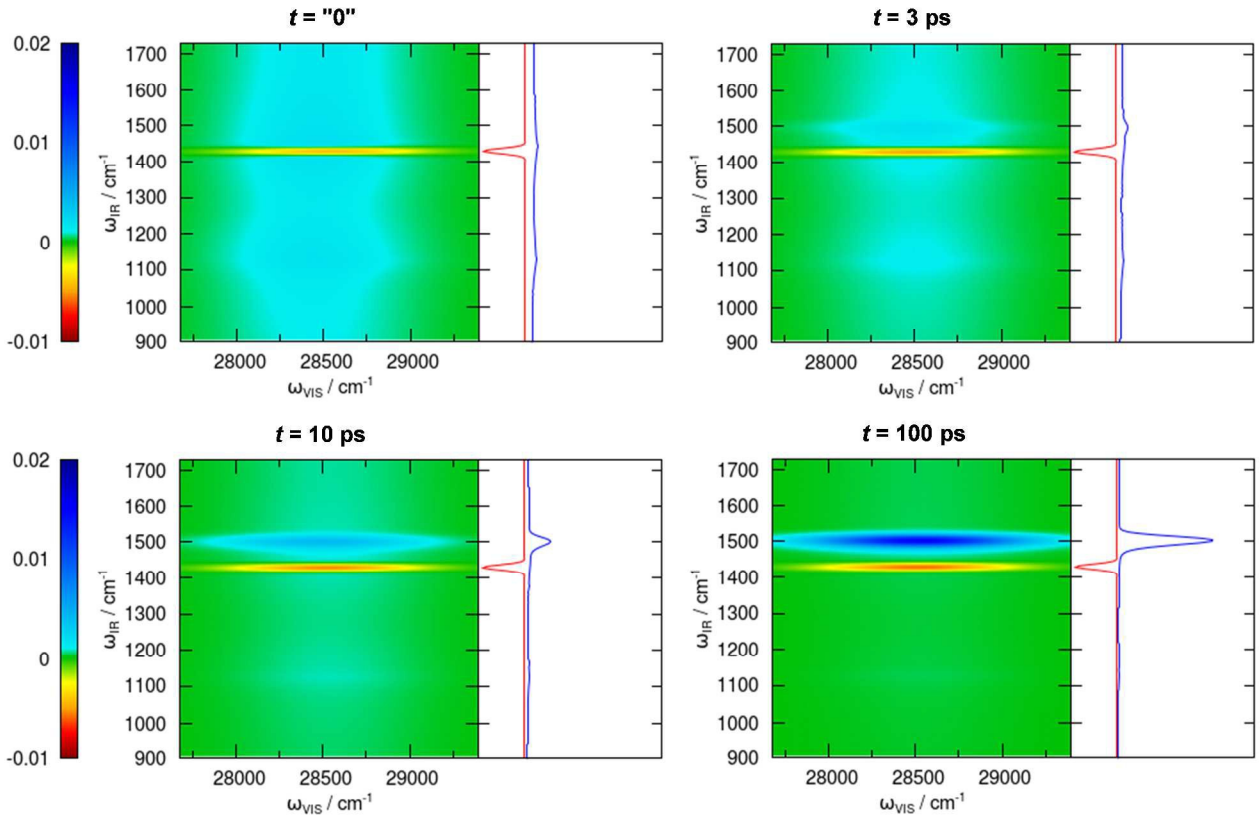

Figure 5. Purely absorptive 2D-EV spectra calculated for AAC in DMSO via the three-state LE/CT model (parameters in Ref. [27]), for the delay times reported on top of each panel. The color maps report the ΔA value according to the palette on the left (arbitrary units). Corresponding 1D spectra are reported along the ω_{IR} axis.

To understand the different shape of 2D-EV spectra calculated for the two dyes, it is important to realize that, upon photoexcitation, AAC reaches a very busy spectral region, where electronic and vibrational excitations have similar energies.[27] In a two-level dye, the IR probe can only excite vibrational transitions, but in AAC it can excite both electronic and vibrational transitions. More precisely, the relevant states of AAC have a mixed LE and CT character and are characterized by a strong nonadiabatic mixing, so that, strictly speaking, it is not even possible to discriminate between electronic and vibrational transitions. This mixing is responsible for broad spectral features, much broader than expected in purely vibrational spectra as observed in DCM (see SI for details about bandwidth assignment). At later times, AAC evolves toward the stable minimum having an almost pure CT character.[27] In this region, the LE-CT energy gap is larger, so that the IR probe only induces vibrational transitions: at long time delays, a more "standard" 2D-EV spectrum is recovered, with sharp photoexcited absorption peaks with almost pure vibrational character.

Very broad 2D-EV spectra are expected for any dye characterized by LE/CT interplay, quite irrespective of model parameters and of the details of the excited-state PES. The broad nature of photoexcited spectra is in fact due to the mixed electronic and vibrational character of excitations in the LE/CT region. Indeed, the LE/CT interplay is effective when the LE and CT states have similar energies, implying strong nonadiabatic mixing with vibrational states. In these conditions, the probe beam in the IR spectral region does not just excite vibrational modes, but addresses mixed electronic and

vibrational states, quite unavoidably leading to broad spectral features (at least at early times).

Conclusions

We presented the first calculation of 2D-EV spectra for charge-transfer dyes, in the framework of essential-state models, taking into account electron-phonon coupling and solvation interaction, including inhomogeneous broadening effects. Solvation dynamics is treated in the framework of the Smoluchowski diffusion equation. Two different cases are discussed, corresponding to (a) a simple push-pull dye with a single relevant excited state, described by a two-state model, and (b) a dye where the LE/CT interplay is captured based on a three-state model. Calculated 2D-EV spectra show a qualitatively different behavior in the two cases, suggesting that 2D-EV spectra offer reliable and detailed information about the nature of excitations. On this basis, the 2D-EV spectra recently reported for DCM in DMSO definitely solve the long-standing debate about the nature of the low-lying excitation(s) in this dye, demonstrating that low-energy spectral properties of DCM are governed by a single excited state, ruling out any LE/CT interplay. The experimental 2D-EV spectra of DCM can be interpreted based on a two-level model accounting for the polarizability of the system, i.e. for the readjustment of the electronic and vibrational structures in response to the evolution of the solvation coordinate. The obtained agreement is impressive, and quantitative discrepancies are inherent to the oversimplified two-state description and limited number of vibrational coordinates. Extending the two-state model to account for other vibrational modes, as well as for other higher-energy electronic states could improve the agreement. On the other hand, for systems with almost degenerate LE and CT states (giving rise to a double-minimum excited-state PES) 2D-EV spectra are expected to have a totally different nature, with the IR pump driving mixed electronic and vibrational excitations, and hence leading to much broader, partially "electronic in nature" spectra along the ω_{IR} axis.

Acknowledgements

Work partially supported by Italian Ministry of Education, University and Research (MIUR) through FIRB (grant RBFR10Y5VW) and PRIN (grant 2012T9XHH7).

Notes and references

[a] Dipartimento di Chimica, Università di Parma & INSTM UdR Parma, Parco Area delle Scienze 17/a, 43124 Parma, Italy.

† Electronic Supplementary Information (ESI) available: details on calculated spectra and theoretical methodology; supplementary 2D-EV spectra. See DOI: 10.1039/b000000x/

1. R. M. Hochstrasser, *Proc. Natl. Acad. Sci. U.S.A.*, 2007, **104**, 14190–14196.
2. M. Cho, *Chem. Rev.*, 2008, **108**, 1331–1418.
3. A. M. Brańczyk, D. B. Turner, and G. D. Scholes, *Ann. Phys.*, 2014, **526**, 31–49.
4. N. T. Hunt, *Chem. Soc. Rev.*, 2009, **38**, 1837–1848.
5. J. M. Anna, C. R. Baiz, M. R. Ross, R. McCanne, and K. J. Kubarych, *Int. Rev. Phys. Chem.*, 2012, **31**, 367–419.
6. T. Brixner, J. Stenger, H. M. Vaswani, M. Cho, R. E. Blankenship, and G. R. Fleming, *Nature*, 2005, **434**, 625–628.
7. N. S. Ginsberg, Y. Cheng, and G. R. Fleming, *Acc. Chem. Res.*, 2009, **42**, 1352–1363.
8. F. Milota, J. Sperling, A. Nemeth, T. Mancal, and H. F. Kauffmann, *Acc. Chem. Res.*, 2009, **42**, 1364–1374.
9. A. Ishizaki and G. R. Fleming, *Annu. Rev. Condens. Matter Phys.*, 2012, **3**, 333–361.
10. K. L. M. Lewis and J. P. Ogilvie, *J. Phys. Chem. Lett.*, 2012, **3**, 503–510.
11. E. Collini, *Chem. Soc. Rev.*, 2013, **42**, 4932–4947.
12. K. L. Wells, P. H. Lambrev, Z. Zhang, G. Garab, and H.-S. Tan, *Phys. Chem. Chem. Phys.*, 2014, **16**, 11640–11646.
13. T. A. A. Oliver, N. H. C. Lewis, and G. R. Fleming, *Proc. Natl. Acad. Sci. U.S.A.*, 2014, **111**, 10061–10066.
14. D. Abramavicius, B. Palmieri, D. V Voronine, F. Sanda, and S. Mukamel, *Chem. Rev.*, 2009, **109**, 2350–2408.
15. G. Hanna and E. Geva, *J. Phys. Chem. B*, 2008, **112**, 12991–3004.
16. C. Olbrich, T. L. C. Jansen, J. Liebers, M. Aghtar, J. Strümpfer, K. Schulten, J. Knoester, and U. Kleinekathöfer, *J. Phys. Chem. B*, 2011, **115**, 8609–8621.
17. A. Halpin, P. J. M. Johnson, R. Tempelaar, R. S. Murphy, J. Knoester, T. L. C. Jansen, and R. J. D. Miller, *Nat. Chem.*, 2014, **6**, 196–201.
18. A. Painelli and F. Terenziani, *J. Phys. Chem. A*, 2000, **104**, 11041–11048.
19. B. Boldrini, E. Cavalli, A. Painelli, and F. Terenziani, *J. Phys. Chem. A*, 2002, **106**, 6286–6294.
20. F. Terenziani, A. Painelli, C. Katan, M. Charlot, and M. Blanchard-Desce, *J. Am. Chem. Soc.*, 2006, **128**, 15742–15755.
21. F. Terenziani, O. V. Przhonska, S. Webster, L. a. Padilha, Y. L. Slominsky, I. G. Davydenko, A. O. Gerasov, Y. P. Kovtun, M. P. Shandura, A. D. Kachkovski, D. J. Hagan, E. W. Van Stryland, and A. Painelli, *J. Phys. Chem. Lett.*, 2010, **1**, 1800–1804.
22. F. Terenziani, C. Sissa, and A. Painelli, *J. Phys. Chem. B*, 2008, **112**, 5079–5087.
23. C. Sissa, V. Parthasarathy, D. Drouin-Kucma, M. H. V Werts, M. Blanchard-Desce, and F. Terenziani, *Phys. Chem. Chem. Phys.*, 2010, **12**, 11715–11727.
24. J. Campo, A. Painelli, F. Terenziani, T. Van Regemorter, D. Beljonne, E. Goovaerts, and W. Wenseleers, *J. Am. Chem. Soc.*, 2010, **132**, 16467–16478.
25. L. Grisanti, C. Sissa, F. Terenziani, A. Painelli, D. Roberto, F. Tessore, R. Ugo, S. Quici, I. Fortunati, E. Garbin, C. Ferrante, and R. Bozio, *Phys. Chem. Chem. Phys.*, 2009, **11**, 9450–9457.
26. C. Katan, M. Charlot, O. Mongin, C. Le Droumaguet, V. Jouikov, F. Terenziani, E. Badaeva, S. Tretiak, and M. Blanchard-Desce, *J. Phys. Chem. B*, 2010, **114**, 3152–3169.
27. C. Sissa, V. Calabrese, M. Cavazzini, L. Grisanti, F. Terenziani, S. Quici, and A. Painelli, *Chem. Eur. J.*, 2013, **19**, 924–935.
28. F. Terenziani, A. Painelli, and D. Comoretto, *J. Phys. Chem. A*, 2000, **104**, 11049–11054.
29. F. Terenziani and A. Painelli, *Chem. Phys.*, 2003, **295**, 35–46.

30. F. Terenziani, M. Morone, S. Gmouh, and M. Blanchard-Desce, *ChemPhysChem*, 2006, **7**, 685–696.
31. F. Terenziani and A. Painelli, *Phys. Rev. B*, 2003, **68**, 165405.
32. A. Painelli and F. Terenziani, *J. Am. Chem. Soc.*, 2003, **125**, 5624–5625.
33. F. Terenziani, S. Ghosh, A.-C. Robin, P. K. Das, and M. Blanchard-Desce, *J. Phys. Chem. B*, 2008, **112**, 11498–11505.
34. F. Terenziani, V. Parthasarathy, A. Pla-Quintana, T. Maishal, A.-M. Caminade, J.-P. Majoral, and M. Blanchard-Desce, *Angew. Chem. Int. Ed.*, 2009, **48**, 8691–8694.
35. M. M. Martin, P. Plaza, and Y. H. Meyer, *Chem. Phys.*, 1995, **192**, 367–377.
36. S. A. Kovalenko, N. P. Ernsting, and J. Ruthmann, *Chem. Phys. Lett.*, 1996, **258**, 445–454.
37. P. van der Meulen, H. Zhang, A. M. Jonkman, and M. Glasbeek, *J. Phys. Chem.*, 1996, **100**, 5367–5373.
38. A. J. Van Tassle, M. A. Prantil, and G. R. Fleming, *J. Phys. Chem. B*, 2006, **110**, 18989–18995.
39. I. D. Petsalakis, D. G. Georgiadou, M. Vasilopoulou, G. Pistolis, D. Dimotikali, P. Argitis, and G. Theodorakopoulos, *J. Phys. Chem. A*, 2010, **114**, 5580–5587.
40. R. S. Fee and M. Maroncelli, *Chem. Phys.*, 1994, **183**, 235–247.
41. M. L. Horng, J. A. Gardecki, A. Papazyan, and M. Maroncelli, *J. Phys. Chem.*, 1995, **99**, 17311–17337.
42. S. Mukamel, *Principles of Nonlinear Optical Spectroscopy*, Oxford University Press, New York, 1995.
43. E. W. Castner, M. Maroncelli, and G. R. Fleming, *J. Chem. Phys.*, 1987, **86**, 1090.
44. M. A. Kahlow, T. J. Kang, and P. F. Barbara, *J. Phys. Chem.*, 1987, **91**, 6452–6455.

